Chemical Physics Letters 664 (2016) 33–38

Contents lists available at ScienceDirect

Chemical Physics Letters

journal homepage: www.elsevier.com/locate/cplett

Research paper

Understanding the light-emitting mechanism of an X-shape organic thermally activated delayed fluorescence molecule: First-principles study

Jianzhong Fan, Lei Cai, Lili Lin *, Chuankui Wang *

Shandong Province Key Laboratory of Medical Physics and Image Processing Technology, School of Physics and Electronics, Shandong Normal University, 250014 Jinan, China

ARTICLE INFO

Article history:
Received 31 July 2016
In final form 4 October 2016
Available online 4 October 2016

ABSTRACT

The light-emitting mechanism of an X-shape organic thermally activated delayed fluorescent molecule is investigated based on first-principles calculations. It is found that there are two stable configurations for the ACRSA molecule, and that the molecule with conformer A is nonluminous. Further, the excited states dynamics of conformer B is studied. The normal modes analysis of the reorganization energy indicates that the non-radiation process of the first singlet excited state (S1) mainly comes from the out-of-plane vibration with low frequencies. Besides, calculations of energy levels of excited states demonstrate that the up-conversion happens between the S1 and T1 states.

1. Introduction

Since the breakthrough of the traditional limit of 25% exciton utilization efficiency in organic light-emitting diodes, the thermally activated delayed fluorescence (TADF) materials arouse people's enthusiasm to develop fluorescent organic light-emitting diodes (OLEDs) with higher efficiency [1–4]. Although much effort has been devoted to this area, efficient TADF materials are still quite rare. Most of these TADF molecules are composed of donor and acceptor groups with steric hindrance between them [5,6]. Because such kind of hindrance can efficiently reduce the orbital overlap between transition orbitals (in most cases, they are the highest occupied molecular orbital and the lowest unoccupied molecular orbital) involved in the first excited states, which can result in a small energy gap between the lowest triplet excited state (T1) and the lowest singlet excited state (S1). The spiro unit, with orthogonally connected π-conjugated element, makes it a useful building block for TADF molecules. Although spiro compounds have been widely studied as emitting materials, there are only three kinds of spiro derivatives have been reported as TADF molecules [7–9]. The X-shape molecule, 10-phenyl-10H,10′-H-spiro[acridine-9,9′-anthracen]-10′-one (ACRSA), that exhibits blue-greenish TADF was reported recently, and it shows an efficient photoluminescence (PL) efficiency of 81% in the solid state and OLEDs with a rather high external quantum efficiency (EQE) of 16.5% [9]. Although the light-emitting mechanism of TADF materials is regarded as the up-conversion of triplet excitons to singlet excitons, the theoretical study of the mechanism of TADF molecules are still quite rare. There are still some doubtful points have not been clarified, such as how the up-conversion being realized, what is the value of the energy gap between the S1 and T1 states, what is the influence of the spin-orbit coupling and other details which cannot be obtained experimentally. In this study, we will perform systematic study on the mechanism of the ACRSA molecule by studying the dynamic process of excitons base on first-principles study. Our theoretical results will provide deep understanding of the mechanism of TADF molecules and also give some helpful insight on the design of high efficient TADF molecules.

2. Theoretical methods

In this paper, the geometry optimizations are performed for the S0 and T1 states by employing density functional theory (DFT) and for S1 state by using the time-dependent density functional theory (TD-DFT) at the B3LYP/6-31G* level. Besides, the frequency calculations are also performed for S0, S1 and T1, which ensures the stabilization of the geometric structures we obtained. Moreover, the vertical excitation energy and adiabatic excitation energy including the zero point vibrational energy (ZPVE) for S0, S1 and T1 are calculated respectively. All these calculations are carried out by GAUSSIAN 09 package [10].

Based on the first-principles calculations, the dynamics of the excited states are also investigated. For convenience, the decay process for the S1 and T1 states are illustrated in Fig. 1. It can be

* Corresponding authors.
E-mail addresses: linll@sdnu.edu.cn (L. Lin), ckwang@sdnu.edu.cn (C. Wang).

http://dx.doi.org/10.1016/j.cplett.2016.10.009
0009-2614/

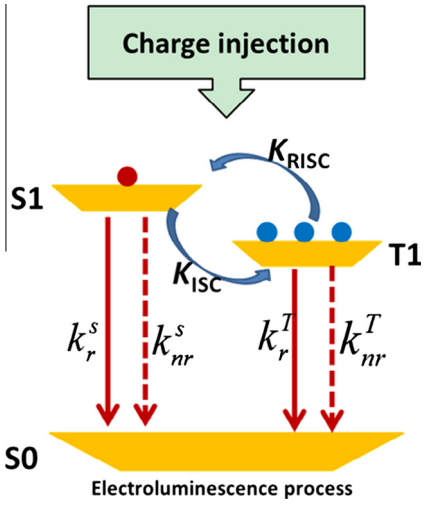

Fig. 1. Electroluminescence process: k_{nr}^S, k_r^S, k_{ISC}, k_{RISC}, k_{nr}^T, k_r^T represents the non-radiative rate from S1, the fluorescence rate, intersystem crossing rate, reverse intersystem crossing rate, non-radiative rate from T1 and phosphorescence rate respectively.

found that there are three kinds of decay pathways for the S1 state, e.g. the radiation, the non-radiation and the intersystem crossing. The decay rates for them are defined as k_r^s, k_{nr}^s and k_{ISC}. For TADF molecules, there are also three pathways to decay for the triplet excitons, the phosphorescence process, the non-radiation process and the reverse intersystem crossing process. The corresponding rates for them are labeled with k_r^T, k_{nr}^T, k_{RISC}. In this paper, the fluorescence rate (or the radiation decay rate of the S1 state) is calculated using the Einstein spontaneous emission rate formula.

$$k_r^S = \frac{f\Delta E^2}{1.499} \tag{1}$$

where f is oscillator strength from S1 state to S0 state, ΔE is the energy difference between the S1 state and the S0 state, which is in the unit of cm^{-1}.

The non-radiation decay of the S1 state and T1 state to the ground state can be evaluated with MOMAP (Molecular Materials Property Prediction Package) [11]. Detail calculation formula can refer to Ref. [12]. The (R)ISC is also one kind of non-radiation decay. To simplicity, the (R)ISC decay rates are calculated with the classical Marcus rate equation [13–15].

$$k_{ji} = \frac{V_{ji}^2}{\hbar}\sqrt{\frac{\pi}{K_B T\lambda}}\cdot \boldsymbol{exp}\left[-\frac{(\Delta G_{ji}+\lambda)^2}{4\lambda K_B T}\right] = \frac{V_{ji}^2}{\hbar}\sqrt{\frac{\pi}{K_B T\lambda}}\cdot \boldsymbol{exp}\left[-\frac{\Delta G^{\perp}}{K_B T}\right] \tag{2}$$

Here, K_B is Boltzmann constant and T is the temperature. V_{ij} is the spin-orbit coupling between the S1 state and the T1 state, and T is the temperature which is set as 300 K here. In the active energy ($\Delta G^{\perp} = \frac{(\Delta G_{ij}+\lambda)^2}{4\lambda}$), ΔG_{ij} is the energy difference between the S1 state and the T1 state and λ is the reorganization involving both the S1 state and T1 state. In calculation of the ISC rate, $\Delta G_{ij} = E_{T1} - E_{S1}$. The parameters involved are all calculated based on the first-principles calculations. The spin-orbit coupling between S1 and T1 is calculated with quadratic response function methods, which can be realized with the Dalton program [16]. In addition, the radiation decay rate of T1 can also be realized in Dalton program, and one can refer to Ref. [17] to see the details.

3. Results and discussions

In our study, the geometric structures of the ground state (S0), the first triplet excited state (T1) and the first excited singlet state (S1) of the ACRSA molecule are first optimized with the density functional theory (DFT) and the timely dependent density functional theory (TD-DFT) at B3LYP/6-31G* level. It is found that there are two local stable structures for the ACRSA molecule in the S0 state. The front view, the top view and the side view for two geometric structures of the ACRSA in S0 state (marked with conformer A and B respectively) are shown in Fig. 2. The acridine moiety as an electron donating unit and the anthracenone moiety as an electron accepting group are perpendicular to each other in both configurations. While the benzene ring connected to the acridine moiety are quite different in two configurations. In conformer A, the benzene ring is perpendicular to the acridine unit and almost parallel with the anthracenone unit, while it has about 70° dihedral angle with the acridine unit and 90° dihedral angle with the anthracenone unit in conformer B. Based on our calculations, we can find that the energy of conformer A is about 0.41 eV lower than B. In Fig. 3, the energy variation of S0, S1 and T1 states with the change of the dihedral angle between the benzene ring and the acridine unit is illustrated. It can be found that there are two stable conformers for all the three states. From the energy potential surface of the molecule (Fig. 3(d)), we can find that the energy barrier for the A changing to B is about 0.398 eV, while it is only 0.006 eV for B changing to A. Consequently, it is quite possible for B changing to A at room temperatures, and conformer A should be the most possible configuration in a stable state. Correspondingly, we can also find two stable conformers for both S1 state and T1 state. The energy surface for the T1 state is quite similar to that of the ground state, the energy barrier for B changing to A is also quite small. Nevertheless, the energy barrier for B changing to A in S1 state is as high as 0.618 eV. The configurations for the S1 state should include conformer B, which is quite important for the emission of the ACRSA molecules. Our calculation indicates that the oscillator strength of the molecule with conformer A in S1 state is zero, which means that conformer A in S1 state does not emit light. Nevertheless, the oscillator strength for conformer B in S1 state is 0.0007 (see Table 1). Although it is quite small, it indicates that the conformer B can still emit light. We conclude that the fluorescent efficiency may be modulated by efficiently controlling the configuration of the molecule in the excited state.

Based on the energy analysis, we deduce that the absorption spectra of the molecule should come from the excitation of conformer A, while the fluorescent spectrum should mainly come from the emission of conformer B. From the experimental results, we can find two absorption peaks with one located at about 300 nm and the other at about 330 nm [9]. From our calculation, we find that the four largest absorption wavelengths for conformer A are 288 nm, 299 nm, 312 nm and 327 nm. For conformer B, the largest two absorption peaks are located at 304 nm and 312 nm. The calculated emission wavelength of conformer B is 508 nm, which also agrees well with the experimental result [9]. The calculated absorption spectra and emission spectra in good agreement with the experimental results further confirm the deduction above.

To study the electroluminescence process, we only focus on the evolution of conformer B, since there is no emission from the S1 state of conformer A. From the energy structure of conformer B (see Fig. 4), we can see that the second singlet excited state is 0.46 eV higher than the S1 state in energy. The lowest two triplet states are close to the S1 state in energy. As the internal conversion process is much faster than the intersystem crossing and the radiation process, we conclude that the intersystem crossing process should mainly happen between the S1 and T1 states for conformer

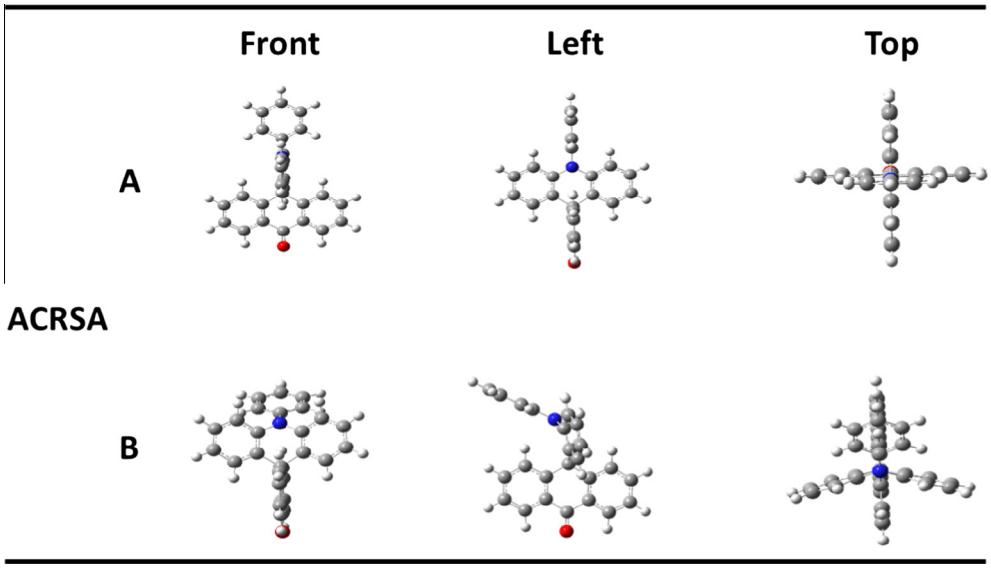

Fig. 2. The front view, top view and side view of conformer A and B of the ACRSA molecule in ground state.

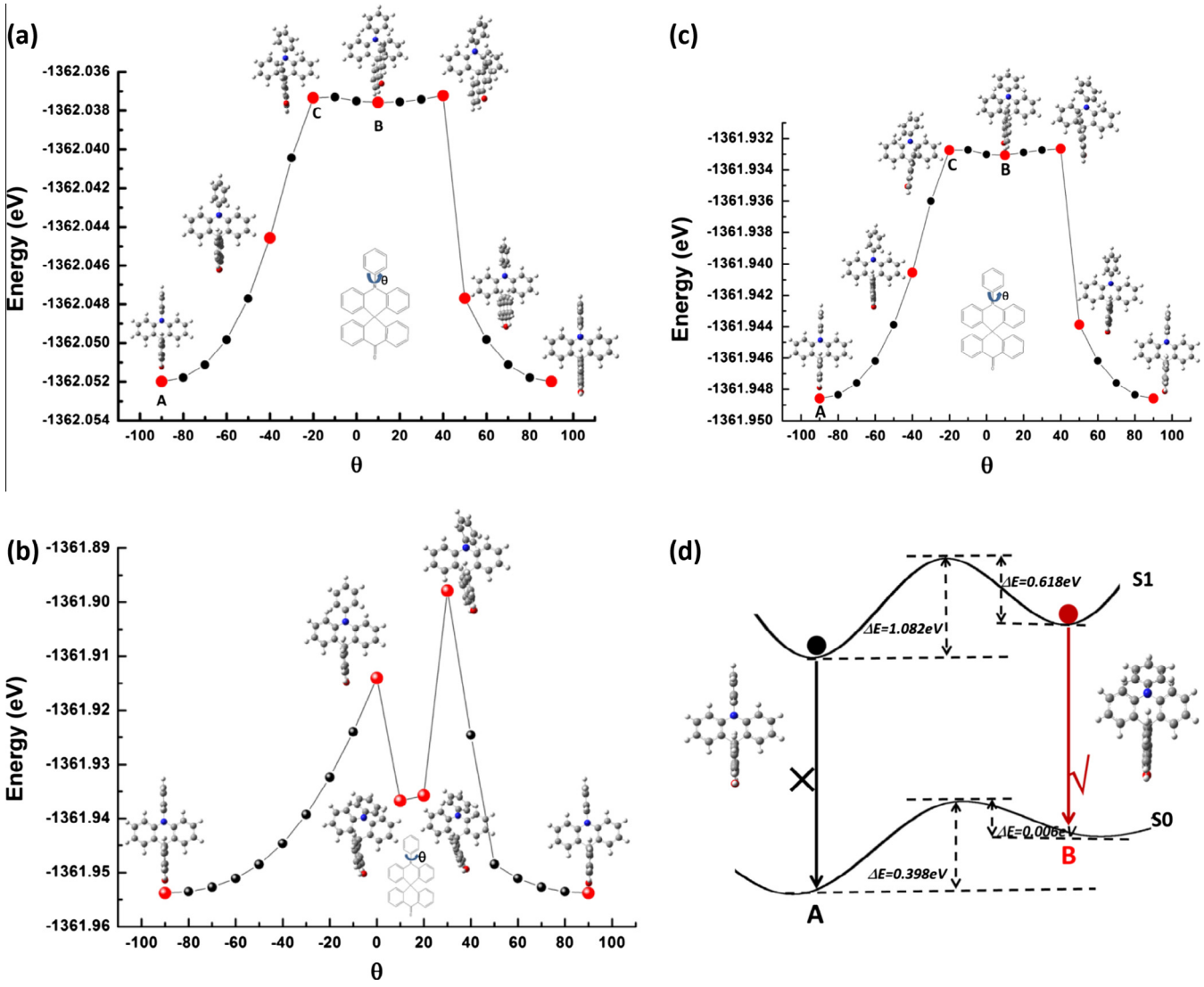

Fig. 3. Potential energy surface for the (a) S0, (b) S1 and (C) T1 state of the ACRSA. The geometric structures with their energy marked with red points are also shown. (d) Schematic picture of energy surface of S1 and S0.

Table 1
Oscillator strength (f), radiation rate (k_r^S) and nonradiative rate (k_{nr}^S) from S1 to S0. k_{ISC} and k_{RISC} is the intersystem crossing and reverse intersystem crossing rate between S1 and T1 respectively. k_r^T and k_{nr}^T is the phosphorescence rate and non-radiative rate from T1 respectively.

	f	k_r^S	k_{nr}^S	k_{ISC}	k_{RISC}	k_r^T	k_{nr}^T
ACRSA	0.0007	1.81×10^5	2.91×10^{10}	6.10×10^4	1.29×10^4	76.5	1.79×10^8

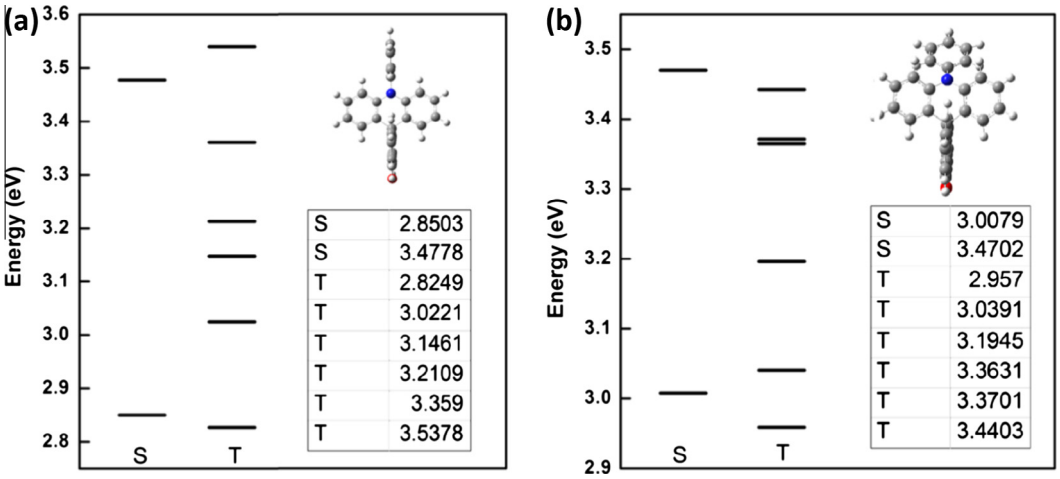

Fig. 4. Molecular energy level diagram of (a) conformer A and (b) conformer B.

B. The calculated decay rate for the S1 and T1 states are listed in Table 1. It can be found that the fluorescent rate for the S1 state is 1.81×10^5 s^{-1}, which is smaller than the fluorescent rate of normal fluorescent materials. This is mainly induced by the weak overlap between transition orbitals (see Fig. 5). From the analysis of electron distribution in molecular orbitals, we can see that the S1 state mainly comes from the contribution of the highest occupied molecular orbital (HOMO) and the lowest unoccupied molecular orbital (LUMO). It can be seen that the electrons mainly distributed on the acridine unit in HOMO and located at the anthracenone unit in LUMO. Weak overlap between transition orbitals is one important way to get a small S1-T1 energy gap,

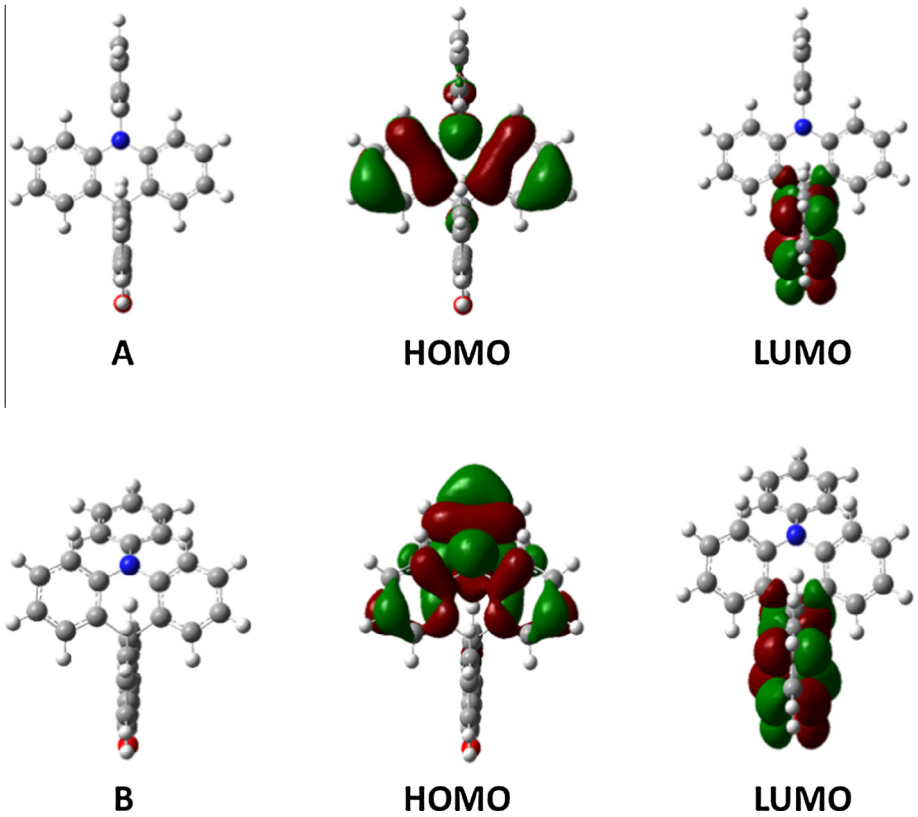

Fig. 5. HOMO and LUMO distributions of conformer A and conformer B.

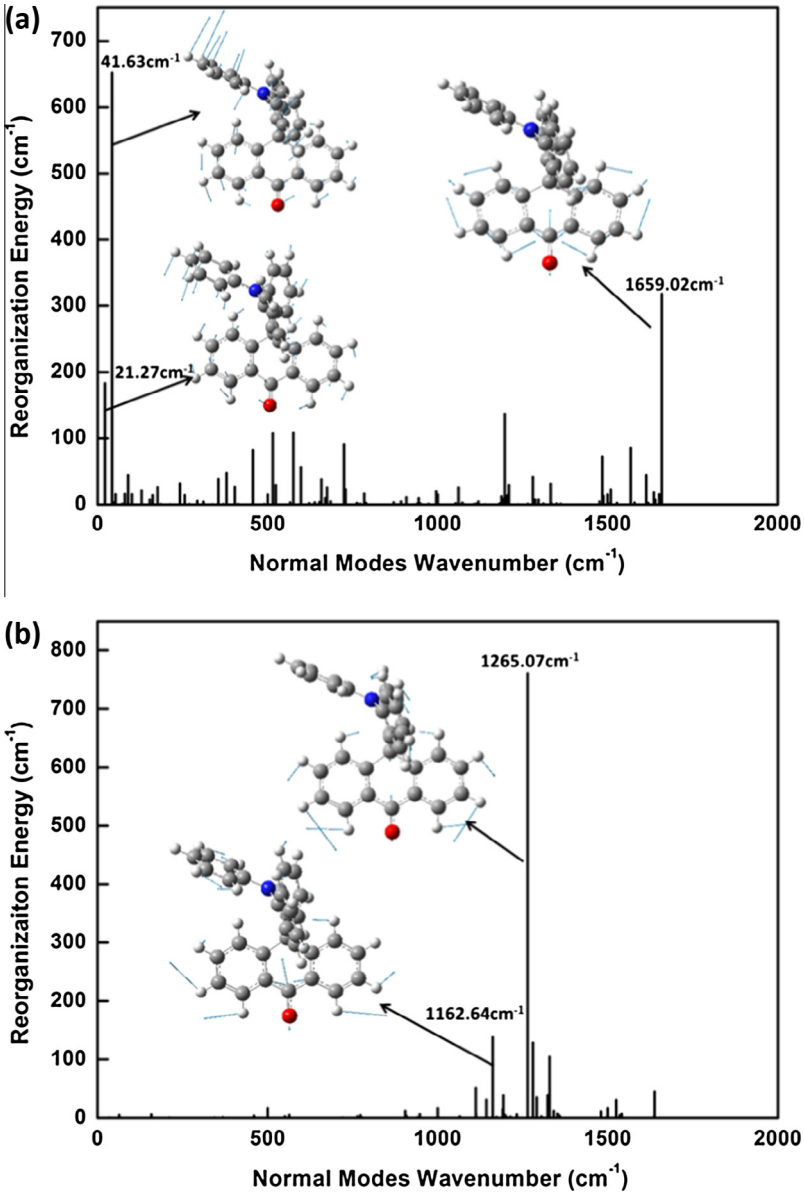

Fig. 6. The normal mode analysis of the reorganization energy for (a) S1 → S0 transition and (b) T1 → S0 transition.

while it can also induce a slow fluorescent rate. For comparison, the energy levels of conformer A are also calculated, which show different structure with conformer B. However, the intersystem crossing should also happens between T1 and S1, which is similar to that of conformer B. The HOMO and LUMO of conformer A are also shown in Fig. 5. It can be found that the electron distributed on both the acridine unit and the benzene rings in the HOMO. It is different with the HOMO of conformer B. This deviation should come from the difference of two conformers. The calculated phosphorescence rate is only 76.5 s^{-1}, while the non-radiation rate of the T1 state is much larger. The non-radiation rate for the S1 state is also quite high, even higher than the radiation rate. From the calculated rates, we should conclude that the ACRSA molecule cannot emit light due to the fast non-radiation rate of the S1 state. However, clear fluorescence is found experimentally. This deviation between theoretical simulations and the experimental results comes from the effect of the environment. In experimental work, the molecule emission is found in the solvent or the film, where the non-radiation rate may be efficiently suppressed [9]. Thus more accurate simulation should be performed by considering the effect of surroundings.

The normal mode analysis of reorganization energy for S1 → S0 transition and T1 → S0 transition is shown in Fig. 6(a) and (b). The vibration modes with largest reorganization energy are also presented. It can be found that the vibration mode at 41.63 cm^{-1} has the largest contribution to the reorganization energy for the S1 → S0 transition, and it is a typical out-of-plane vibration. In addition, the vibration mode at 21.27 cm^{-1} with out-of-plane wagging and the mode at 1659.02 cm^{-1} with in-plane bending also contribute the reorganization energy to large extent. In OLEDs, the vibrations with low frequency will be efficiently suppressed due to the concentrated distribution of molecules [18], which implies that the two vibrations at 21.27 cm^{-1} and 41.63 cm^{-1} will have little contribution to the reorganization energy. Consequently, the non-radiation will be suppressed, since the non-radiation process can also be seen as an energy reorganization process. For the T1 → S0 transition, the vibration mode at 1265.07 cm^{-1} has the dominant contribution to the reorganization

energy. In addition, other modes around 1200 cm^{-1} have also some contribution, and all these modes are in-surface bending modes. As the vibration frequencies of these modes are relatively high, they will not be influenced significantly when molecules are prepared in OLEDs. Thus the non-radiation process of the T1 state will not be efficiently suppressed, and it should be the main decay process for T1 state in OLEDs.

The intersystem crossing rate from S1 to T1 and the reverse intersystem crossing rate from T1 to S1 are $6.1 \times 10^4\ s^{-1}$ and $1.29 \times 10^4\ s^{-1}$ respectively. As we know, the intersystem crossing rate is proportional to the spin-orbit coupling and in reverse proportion to the energy gap between two states. The calculated S1-T1 energy gap is 0.05 eV, which is in consistent with the experimental deduction (0.03 eV for doped film or 0.04 eV for the neat film) [9]. However, the calculated spin-orbit coupling is as small as 0.05 cm^{-1}. That is the reason why the intersystem crossing rate is also quite small. Based on our calculation, we conclude that one should also pay attention to the spin-orbit coupling between the S1 and T1 state besides the S1-T1 energy gap. Although the S1-T1 energy gap is quite small, the spin-orbit coupling should be large enough to ensure an efficient (reverse) intersystem crossing.

To confirm our deduction that the molecules around the emitters may play an important role in the light-emitting of the fluorescent emitters, the photophysical properties of the ACRSA molecule in solid state are investigated by using hybrid quantum mechanics and molecular mechanics (QM/MM) method with detail calculation method in the electronic supplementary material. The energy levels of several low-lying excited states of the ACRSA molecule in solid state are plotted in Fig. S2. It can be found that the S1-T1 energy gap is 0.02 eV, which is smaller than that calculated in gas phase. Thus a larger RISC rate between S1 and T1 is expected. In addition, the vibrational contribution to the reorganization energy from S1-S0 is analyzed as shown in Fig. S3. It can be seen that the vibration modes with low frequencies contributes only a little to the reorganization energy, which is quite different with that calculated in gas phase (see Fig. 6(a)). It means that the vibration modes with low frequencies are effectively suppressed in the solid state due to the steric hindrance of the surroundings. The non-radiative rate calculated in solid state is $9.83 \times 10^6\ s^{-1}$, which is about 4 orders magnitude smaller than that calculated in gas phase. To confirm the reliability of the nonradiative rate in our calculation, we plot the $\log K_{nr}^S$ ($\Delta E(eV)$) parabola in Fig. S4. No vibrational feature is found in the curve, which indicates the accuracy of the calculation. Although the radiative rate calculated in solid state ($3.46 \times 10^4\ s^{-1}$) is a little smaller than that calculated in gas phase, the theoretical fluorescent efficiency agrees better with the experimental results than that calculated in gas phase. It indicates the important effect of the environment in the theoretical simulation of the light-emitting properties of fluorescent emitters in OLEDs.

4. Conclusions

In conclusion, two kinds of stable structures are theoretically found for the ACRSA molecule, and conformer A is more stable than conformer B. Calculation also indicates that the molecule with conformer B is responsible for the fluorescence emission, since conformer A has no radiation. In addition, the dynamics of the S1 state in conformer B is investigated, which indicates that the radiation rate is relatively smaller than normal fluorescent emitters. The dynamic calculations of excited states performed in the gas phase shows that the non-radiation process is much faster than the radiation process, which is in poor agreement with the experimental results. The out-of-plane vibration modes are found to contribute most to the reorganization energy of S1. They are effectively suppressed in our simulation performed in solid phase, and both the reorganization energy and the non-radiation rate is significantly reduced. The theoretical calculations in solid state agree better with the experimental results than that performed in gas phase, which indicates the important effect of the environment in theoretical simulations. Besides, the calculation of energy levels of excited states demonstrates that the up-conversion happens between the T1 state and the S1 state, which further confirms the TADF mechanism of the ACRSA molecule.

Acknowledgments

This work is supported by the National Science Foundation of China (Grant Nos. 11374195 and 21403133). Thanks to the supporting of Taishan Scholar Project of Shandong Province and the Scientific Research Foundation of Shandong Normal University. Thanks to the supporting of the Promotive Research Fund for Excellent Young and Middle-aged Scientists of Shandong Province (Grant No. BS2014CL001) and the General Financial Grant from the China Postdoctoral Science Foundation (Grant No. 2014M560571). Great thanks to Professor Yi Luo and Tian Lu for their helpful suggestions and discussions in the detail calculations. Thanks to Professor Yingli Niu for the usage of MOMAP.

Appendix A. Supplementary material

Supplementary data associated with this article can be found, in the online version, at http://dx.doi.org/10.1016/j.cplett.2016.10.009.

References

[1] H. Uoyama, K. Goushi, K. Shizu, H. Nomura, C. Adachi, Nature 492 (2012) 234–238.
[2] Q.S. Zhang, B. Li, S.P. Huang, H. Nomura, H. Tanaka, C. Adachi, Nat. Photon. 8 (2014) 326–332.
[3] H. Tanaka, K. Shizu, H. Nakanotani, C. Adachi, J. Phys. Chem. C 118 (2014) 15985–15994.
[4] K. Shizu, H. Noda, H. Tanaka, M. Taneda, M. Uejima, T. Sato, K. Tanaka, H. Kaji, C. Adachi, J. Phys. Chem. C 119 (2015) 26283–26289.
[5] Q.S. Zhang, J. Li, K. Shizu, S.P. Huang, S. Hirata, H. Miyazaki, C. Adachi, J. Am. Chem. Soc. 134 (2012) 14706–14709.
[6] M. Aonuma, S.H. Wu, Q.S. Zhang, S.P. Huang, T. Nakagawa, K. Kuwabara, C. Adachi, J. Mater. Chem. C 2 (2013) 421–424.
[7] T. Nakagawa, S. Ku, K. Wong, C. Adachi, Chem. Commun. 48 (2012) 9580–9582.
[8] G. Mehes, H. Nomura, Q. Zhang, T. Nakagawa, C. Adachi, Angew. Chem. Int. Ed. Engl. 51 (2012) 11311–11315.
[9] K. Nasu, T. Nakagawa, H. Nomura, C.J. Lin, C.H. Cheng, M.R. Tseng, T. Yasuda, C. Adachi, Chem. Commun. 49 (2013) 10385–10387.
[10] G.W.T.M.J. Frisch, H.B. Schlegel, G.E. Scuseria, J.R.C.M.A. Robb, G. Scalmani, V. Barone, B. Mennucci, H.N.G.A. Petersson, M. Caricato, X. Li, H.P. Hratchian, J.B. A.F. Izmaylov, G. Zheng, J.L. Sonnenberg, M. Hada, K.T.M. Ehara, R. Fukuda, J. Hasegawa, M. Ishida, T. Nakajima, O.K. Y. Honda, H. Nakai, T. Vreven, J.A. Montgomery Jr., F.O.J.E. Peralta, M. Bearpark, J.J. Heyd, E. Brothers, V.N.S.K.N. Kudin, R. Kobayashi, J. Normand, A.R.K. Raghavachari, J.C. Burant, S.S. Iyengar, J. Tomasi, N.R.M. Cossi, J.M. Millam, M. Klene, J.E. Knox, J.B. Cross, C.A.V. Bakken, J. Jaramillo, R. Gomperts, R.E. Stratmann, A.J.A.O. Yazyev, R. Cammi, C. Pomelli, J.W. Ochterski, K.M.R.L. Martin, V.G. Zakrzewski, G.A. Voth, J.J.D.P. Salvador, S. Dapprich, A.D. Daniels, J.B.F.O. Farkas, J.V. Ortiz, J. Cioslowski, D.J. Fox, Gaussian Inc, Wallingford CT, 2009.
[11] G. Shuai, Q. Peng, Y.L. Niu, H. Geng, MOMAP, A Freeand Open-Source Molecular Materials Property Prediction Package; Revision 0.2.004, Shuai Group, Beijing, 2014. <http://www.shuaigroup.net/>.
[12] Q. Peng, Y.L. Niu, Q.H. Shi, X. Gao, Z.G. Shuai, J. Chem. Theory. Comput. 9 (2013) 1132–1143.
[13] R.A. Marcus, J. Chem. Phys. 24 (1956) 966–978.
[14] R.A. Marcus, Rev. Phys. Chem. 15 (1964) 155–196.
[15] R.A. Marcus, Rev. Mod. Phys. 65 (1993) 599–610.
[16] Dalton, A Molecular Electronic Structure Program <http://daltonprogram.org>.
[17] K. Aidas, C. Angeli, K.L. Bak, et al., The Dalton quantum chemistry program system, Wiley Interdisc. Rev., Comput. Mol. Sci. 4 (2014) 269–284.
[18] C.M. Deng, Y.L. Niu, Q. Peng, A.J. Qin, Z.G. Shuai, J. Chem. Phys. 135 (2011) 014304.